Hydraulic characterization of unconfined aquifers with oscillatory excitations: A numerical analysis

Pierre Fischer, Abderrahim Jardani

Research Paper/

Hydraulic Characterization of Unconfined Aquifers with Oscillatory Excitations: A Numerical Analysis

P. Fischer[1], A. Jardani[2]

(1) HydroSciences Montpellier, Univ. Montpellier, CNRS, IRD, Montpellier, France

(2) Normandie Univ, UNIROUEN, UNICAEN, CNRS, M2C, 76000 Rouen, France

Conflict of interest: None

Corresponding author: P. Fischer

E-mail : pierre.fischer@umontpellier.fr

Key words: Van Genuchten, Periodic signal, Imaging, Subsurface, Tomography, Vadose zone

Intended for publication in Journal of Hydrology

Abstract

We present a synthetic hydraulic analysis of the propagation of oscillatory perturbations in a two-dimensional saturated zone bounded above by a capillary fringe. Unsaturated flows are simulated in a physical model using a hysteretic form of Richards' equation parameterized using the van Genuchten water retention curve and the Mualem hydraulic conductivity equation for a sand, loam, and intermediate soil. Soil type affects periodic responses as a function of their hydrodynamic and van Genuchten properties. We first analyze the effect of various hydraulic or signal properties on the oscillatory responses simulated at different locations and depths. We then test the imaging potential of oscillatory responses recorded in the saturated zone to spatially charaterize homogeneous or heterogeneous soils, also considering the effect of period of oscillation. We find that a separation of these responses into amplitude/phase couples permits to dissociate the characterization of different hydraulic properties. Periodic amplitudes decay with distance mainly as a function of hydraulic conductivity and phase lags decrease with frequency due to storage in the capillary fringe. Thus, responses amplitude appears to be especially sensitive to conductivity K, which allows to isolate this property from the others. Phases can then be used to better characterize the vertical flows effect, through the Van Genuchten parameters α and n. Higher periods will tend to accentuate the unsaturated flows effect on the responses and can therefore be adopted for a better characterization of α and n. However, using low-period responses can also be useful, as they provide better estimates of conductivity values in media with low heterogeneities. We consider this work as a useful preliminary analysis for future sandbox or field real cases applications and provide advices for such applications in the discussion.

1. Introduction

In hydraulic characterization of unconfined aquifers by pumping tests, identifying the impact of the capillary fringe on saturated flows remains a non-trivial task. Indeed, the unsaturated zone can contribute substantially to the flows in the saturated zone through vertical fluxes (Neuman 1972; Mishra et al. 2012; Lin et al. 2017). Therefore, a rigorous interpretation of these tests requires a quantification of these vertical fluxes and a characterization of the hydraulic properties of the unsaturated zone. In addition, a spatial characterization of the hydraulic properties (such as hydraulic conductivity) of unconfined aquifer including its cover can substantially improve our comprehension of the processes of recharge and contaminant transport in the critical zone. This can be performed with a hydraulic tomography approach in which a physical numerical model is used in an inversion process to retrieve the hydraulic properties by fitting hydraulic head measurements. Usually, in such approach, these hydraulic heads are measured simultaneously in multiple wells and at multiple depths in response to cross-wells perturbations (Yeh and Lee 2007; Yeh et al. 2013; Liu et al. 2002; Zhu and Yeh 2005).

In the literature, several hydraulic tomography of unconfined aquifers have already been performed on field or laboratory applications. In particular on field cases applications, the Boise Hydrogeophysical Research Site (BHRS), has been particularly studied (Cardiff et al. 2009; Cardiff and Barrash 2011; Cardiff et al. 2012; Cardiff et al. 2013a; Rabinovich et al. 2015; Hochstetler et al. 2016; Cardiff et al. 2019). However, in these applications, the authors considered that the drainage occurring during their tests was instantaneous and did not generate delayed responses effect. Thus, they simulated only the saturated flows in the aquifer in order to characterize the conductivity and specific storage fields. It is shown that this approximation is acceptable when a specific yield value is employed for the drainage in the early-time pumping (Cardiff and Barrash 2011; Cardiff et al. 2012). However, to apply this

method, the effective porosity must trigger instantaneous drainage at the beginning of the pumping or the effective porosity must contribute only for a negligible vertical flux compared to the horizontal fluxes generated by pumping (Cardiff and Barrash 2011). Mao et al. (2013a) have presented a theoretical analysis of the application of hydraulic tomography on an unconfined aquifer also taking into account hydraulic properties related to the unsaturated flows (pore-size distribution parameters and saturated water content). This approach has been successfully applied theoretically and experimentally in sandboxes with an analysis of temporal drawdown curves in response to constant-rate pumping (Mao et al., 2013b; Zhao et al. 2015).. However to date a real field case application following this method has not been presented. Therefore further recommendations have been provided for adapting such process in real applications in Mao et al. (2013a) and Zhao et al. (2015). The major concerns in its application remains effect of noise on the data and the necessity to assess a sufficient amount of information on both the saturated flows (rather horizontal) and the unsaturated flows (rather vertical) in the dataset.

Oscillatory pumping tests can improve the quality of hydraulic data and thus the characterization of unconfined aquifers, including the effect of the marginal capillary zone. During the last decades, applications of oscillatory excitations in the identification of the hydraulic properties of aquifers have been widely explored, both theoretically and experimentally (Black and Kipp 1981; Rasmussen et al. 2000; Rasmussen et al. 2003; Renner and Messar 2006; Fokker et al. 2013; Fischer et al. 2018; Salina Borello et al. 2019; Cardiff et al. 2019; Fischer et al. 2020a; Fischer et al. 2020b). The imaging potential of such data has been studied in Cardiff et al. (2013b) and their advantages in field application have been discussed in Bakhos et al. (2014) in terms of ability to easily eliminate noises from the measurements and in Cardiff and Barrash (2014) for configuring the period of oscillation in order to investigate different flowpaths in the aquifer.

The propagation of oscillatory signals in soils under conditions of variable saturation has been analyzed in several works with numerical data (Revil et al. 2008; Shoushtari et al. 2015) or laboratory data (Cartwright et al. 2003; Cartwright et al. 2004; Cartwright 2014). All these works discuss the effect of hysteresis, existing for unsaturated flows and having an impact on the oscillatory responses. This hysteresis effect is due to the wetting and dewatering processes of soils that generate loops in the water content curves. These scanning loops can be modeled with hydrodynamic-dependent unsaturated flows parameters. Effects of air entrapment during soils wetting, can also temporarily affect the saturated water content value (Kool and Parker 1987).

Several analytical solutions have recently been proposed for the estimation of soils hydraulic property values in unconfined aquifers from oscillatory signal responses (Dagan and Rabinovich 2014; Huang et al. 2018; Huang et al. 2019; Cheng and Renner 2018). However, it is still rare for spatial variability to be taken into account in characterization applications considering both the saturated and unsaturated hydraulic properties. Furthermore the information brought by oscillatory responses for the spatial characterization of unconfined aquifers still needs to be investigated. With this work our aim is to further investigate the effect of oscillatory flows generated at the limit of the saturated zone in an unconfined aquifer, in order to propose a preliminary analysis of this type of data for future characterization application, in particular hydraulic tomography. For this purpose we simulated flows associated to extraction/injection oscillations in a synthetic sandbox with a physical numerical model. We first present an analysis of the effect of different soil properties on the oscillatory responses. Then we focus more particularly on the effect of conductivity K and the unsaturated Van Genuchten parameters α and n and study the possibility to spatially characterize these properties with the information carried in the oscillatory

97 responses. Finally we discuss our analysis and imaging results in order to provide some
98 advices for future works of hydraulic tomography using this type of data.

99 2. Presentation of the model

100 We developed a physics-based model of an unconfined soils with variable saturation with
101 COMSOL Multiphysics (see Figure 1). This model represents a 2-D side-views of a synthetic
102 sandbox at a metric scale: 3m wide for 1m depth. We considered the initial water table to be
103 50 cm below the surface (thus, initially, half of the model is saturated and the other half
104 unsaturated). The modeled sandbox is equipped with a pumping/injection point (hereafter
105 noted S) and measurement axes at distances of 20, 40 and 60 cm from the pumping axis, in
106 which hydraulic pressure responses are simulated at different depths of the saturated zone (60
107 and 90 cm).

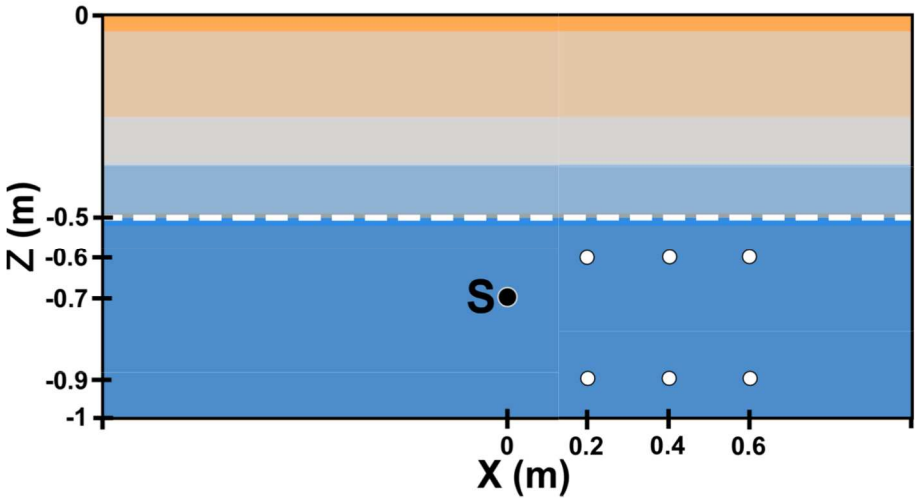

108

109 Figure 1: Schematic representation of our side-viewed models of an unconfined aquifer.
110 Surface is at $Z = 0$ cm and the water table at $Z = -50$ cm. The white circles represent the
111 pressure simulations points while the black circle represents the perturbation source point
112 (also used as pressure measurement). Orange color represents the soil, light blues the
113 unsaturated fringe and blue the saturated zone of the aquifer.

114

In order to take into account the capillary fringe effect on the saturated responses, we simulated water flows with Richards' formulation of the continuity equation for a 2D side-viewed temporal model:

$$\left(C_m + S_e.S\right)\frac{\partial h}{\partial t} + \nabla.\left(-K.k_r\left(\nabla H_p + \nabla z\right)\right) = q \ , \qquad (1)$$

where t is time (s), H_p is the hydraulic pressure (m) at a given depth z (m), K is the hydraulic conductivity (m/s), S is the storage coefficient (m^{-1}) related to the soil compressibility, S_e denotes the effective saturation (-), C_m is the specific moisture capacity (m^{-1}), k_r is the relative permeability (-) and q is the Darcy's velocity at the pumping locations (m/s). We consider that no vertical flows occur at the upper boundary of the sandbox during the simulations. The other boundaries are impervious, implying a finite volume of water in the sandbox (no inlet or outlet). The flows in the model are then solved within an adaptive-size triangular mesh with a finite-element method.

This model simulates, in time, the hydraulic pressures in the variably saturated soil in response to a sinusoidal oscillating perturbation, injecting and extracting successively a same amount of water.

$$Q = -Q_A.sin\left(\frac{2.\pi}{Pe}.t\right) \qquad (2)$$

where Q is the extraction/injection flowrate (m^3/s), Q_A is the oscillating flowrate amplitude (m^3/s) and and Pe is the oscillating flowrate period (s).

S_e, C_m and k_r are calculated with the Van Genuchten equations. These equations are dependent on the groundwater pressure $H_p = h - z$; i.e. if the water, at a given location (x,z), is at an atmospheric pressure or not:

136
$$\begin{cases} S_e = \dfrac{1}{\left(1+\left|\alpha.H_p\right|^n\right)^{1-1/n}} & \text{if } H_p < 0 \\ S_e = 1 & \text{if } H_p \geq 0 \end{cases} \quad (3)$$

137
$$\begin{cases} C_m = \dfrac{\alpha\left(1-\dfrac{1}{n}\right)}{1+\dfrac{1}{n}}.(\theta_s-\theta_r).S_e^{\frac{1}{1-1/n}}.\left(1-S_e^{\frac{1}{1-1/n}}\right)^{1-1/n} & \text{if } H_p < 0 \\ C_m = 0 & \text{if } H_p \geq 0 \end{cases} \quad (4)$$

138
$$\begin{cases} k_r = S_e^{\ell}.\left(1-\left(1-S_e^{\frac{1}{1-1/n}}\right)^{1-1/n}\right)^2 & \text{if } H_p < 0 \\ k_r = 1 & \text{if } H_p \geq 0 \end{cases} \quad (5)$$

139 where α (m^{-1}), n (-) and $\ell = 0.5$ (-) are the Van Genuchten parameters and θ_s, θ_r are the
140 saturated and residual water content (-).

141 A hysteretic effect occurs in unsaturated soils, inducing a difference in the dewatering and the
142 wetting of the soil. In this study, a spatial and temporal frequency-dependent hysteresis effect
143 is implemented in the model, based on the formulation of Revil et al. (2008) for periodic
144 sources and the observations made in Shoushtari et al. (2015) that hysteresis effects attenuates
145 with distance to the signal source. The hysteresis is generated by computing dynamic values
146 of α and n, following the induced periodic movement, over space and time:

147
$$\alpha(t) = \alpha_{mean} \times \left[1-\left(M_{hyst} - min\left(\frac{\left|z_p - z\right|}{z_{hyst}},1\right).M_{hyst}\right).sin\left(\frac{2\pi t}{Pe}\right)\right] \quad (6)$$

148 where M_{hyst} is the magnitude of the hysteresis effect (%), α_{mean} represents the mean value of
149 α (1/m), z_p is the pumping depth (m) and z_{hyst} is the distance of attenuation of the hysteresis

150 effect (hereafter 50 cm). A similar formulation is also used to compute $n(t)$, considering a
151 n_{mean} value (-).

152 We briefly present in Figure 2 the effects of the simulated hysteresis on the saturation level
153 and the simulated pressures in our model. After one cycle of pumping/injection the saturation
154 level will not come back to its origin when incorporating a hysteresis effect. A part of the
155 mobilized water will remain in the unsaturated zone, generating a lowering of the saturation
156 level. After several cycle, the effect generates a global decrease of the saturated/unsaturated
157 interface. In the unsaturated zone, the shape of the signal becomes deformed by the hysteresis
158 effect (especially observable for the period of 30 min), wherein it cannot be considered as a
159 sinusoidal form anymore. The effect of the period of oscillation is also more important in the
160 unsaturated zone, where the oscillatory response tends to vanish faster (in terms of amplitude)
161 than in the saturated zone when the period of the signal is decreased. In the saturated zone, the
162 hysteresis effect does not seem to modify the shape of the signal directly. Thus the pressure
163 responses in the saturated zone contain a sinusoidal part (h_{osc}) in response to the oscillating
164 signal that can be written:

165 $$h_{osc} = h_A . sin\left(\frac{2.\pi}{Pe}.t - h_P.\frac{\pi}{180}\right) \quad (7)$$

166 where h_A is the oscillating response amplitude (m) and h_P is the oscillating response phase
167 lag to the signal source (°).These oscillatory parts can be extracted from the head responses
168 through a Fast Fourier Transform (FFT) directly in terms of timeless amplitudes (h_A) and
169 phases (h_P).

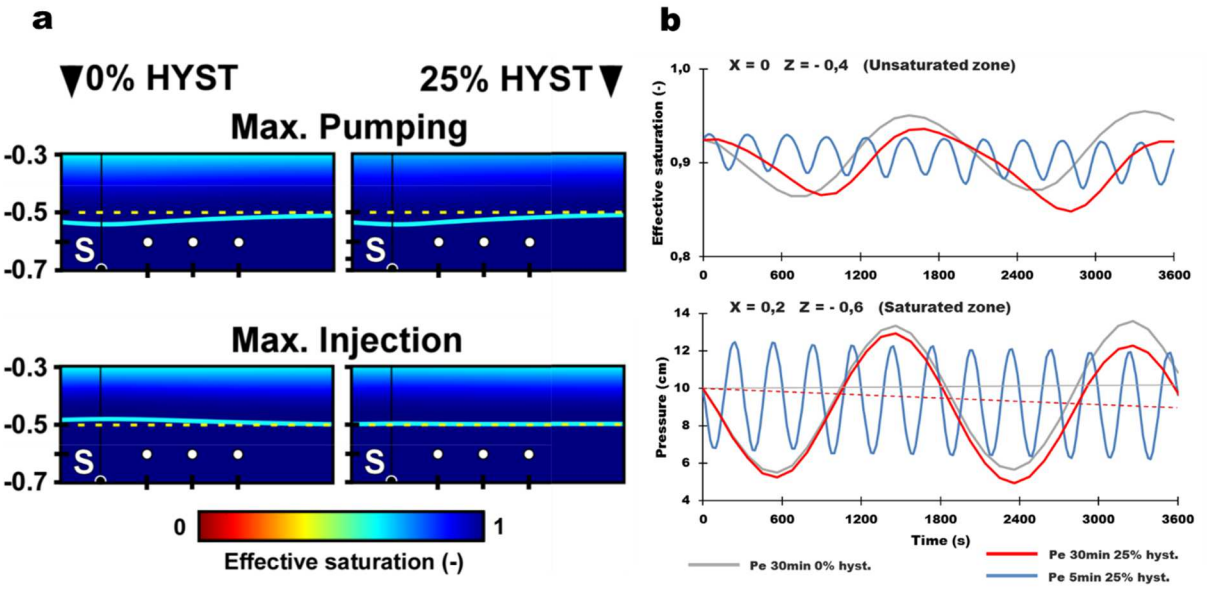

Figure 2: (a) Effect of simulated 25% hysteresis on the soil effective saturation and the saturation level (cyan line) during one cycle of pumping and injection. The initial saturation level is indicated as a dotted line. (b) Effect of the hysteresis on the effective saturation simulated at position (0;-0.4) in the unsaturated zone and the pressure simulated at position (0.2;-0.6) in the saturated zone after several cycles of injection/pumping and for different periods of oscillation (5 and 30 min)

We simulated and observed the oscillatory responses in the saturated zone for different types of soils, by modifying the property values inputs in the model. Hereafter in this work we principally compare these responses in sand, in loam or an intermediate soil with properties between sand and loam ones. The hydraulic property values employed for these two configurations are presented in Table 1 and were chosen mainly according to the UNsaturated SOil hydraulic DAtabase (UNSODA) in Leij et al. (1996) and to previous works in the unconfined aquifers literature.

187 Table 1: Property values used in our model for the two types of soils and the intermediate soil
188 considered.

	K (m/s)	Anisotropy (Kx / Kz)	α (1/m)	n (-)
'Loam' soil	1.10^{-5}	4	3.2	2.4
'Intermediate' soil	5.10^{-5}	3	4.0	2.7
'Sand' soil	1.10^{-4}	2	5.0	3.0

189

190 For the hydrogeological soil properties we chose constant values, also based on what can be
191 usually found in the literature: $\theta_r = 0.05$, $\theta_s = 0.40$ and $S = 10^{-5}$ m^{-1}. We considered a M_{hyst} =
192 25 % magnitude hysteresis effect in the unsaturated zone, based on the recommendations in
193 Kool and Parker (1987).

194 Figure 3 presents the differences between our simulated sand and loam soils in terms of
195 unsaturated flows (i.e. effective saturation profiles, water content curves and hysteresis effects
196 on the responses in the saturated zone). It can be noted that this hysteresis effect, shown in
197 Figure 2, is more important in sand than in loam.

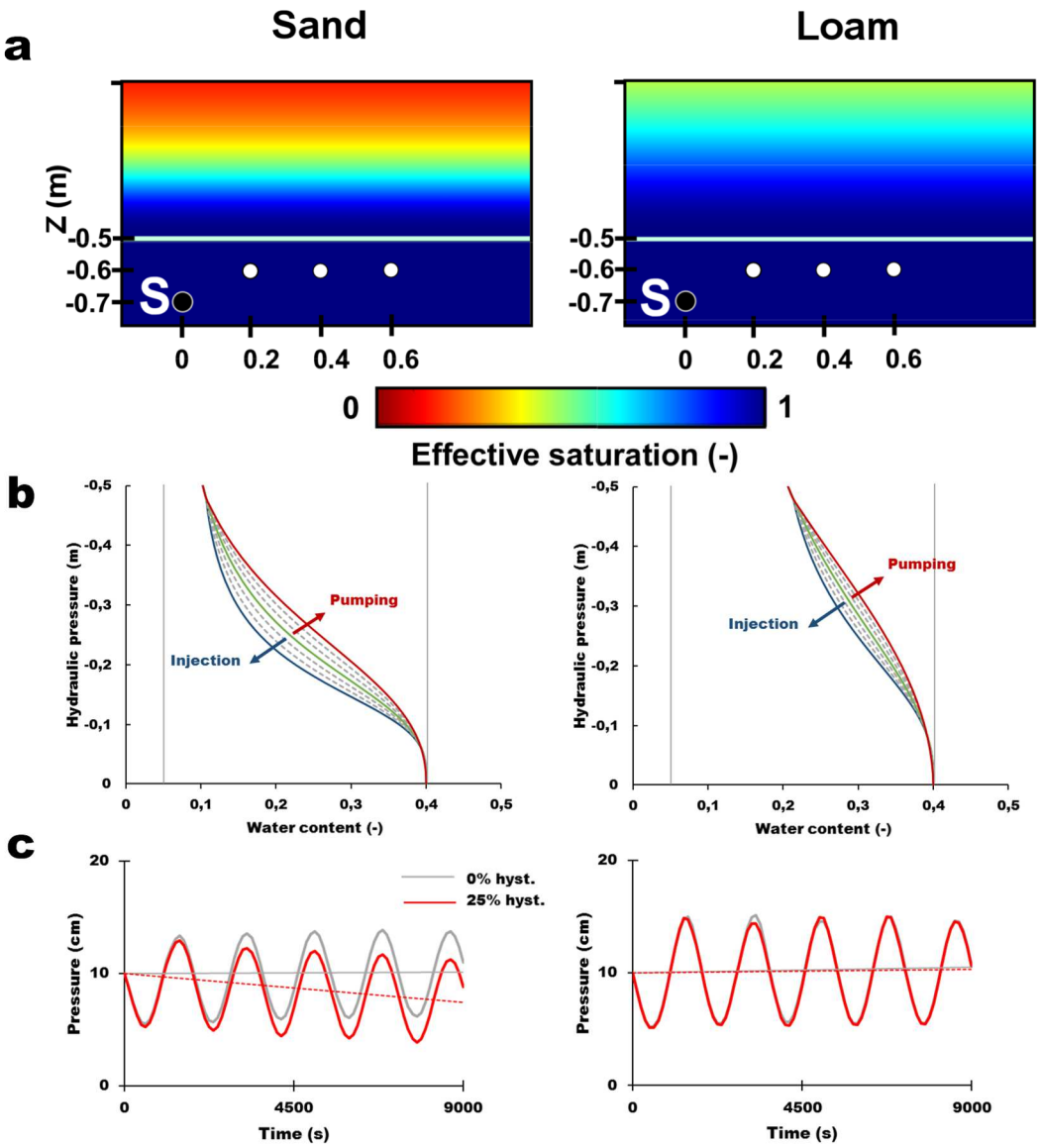

Figure 3: (a) Effective saturation in sand and loam between the surface and the saturated zone, at 50cm depth. (b) A spatial and temporal-evolving hysteresis effect ('scanning loop') has been taken into account in the water content curves during the successive pumping and injection phases. (c) This hysteresis effect does not substantially affect the oscillation response, but rather the mean pressure level, especially in sands (here the pressures simulated at position (0.2;-0.6) with 0% and 25% hysteresis effects for a period of oscillation of 30 min).

3. Comparative analysis of the effect of various soil properties on the oscillatory responses

By simulating flows during pumping and injection phases in sand and loam (Figure 4), we can clearly observe the different types of flows that will be mobilized in these two configurations. Vertical flows will occur in the unsaturated zone, horizontal in depths of the saturated zone, and mixed vertical/horizontal flows near the saturated/unsaturated interface. It can also be observed from the arrows sizes (proportional to the flow intensity) in the unsaturated zone in Figure 4 that vertical flows are, in proportion, more important in sand than in loam.

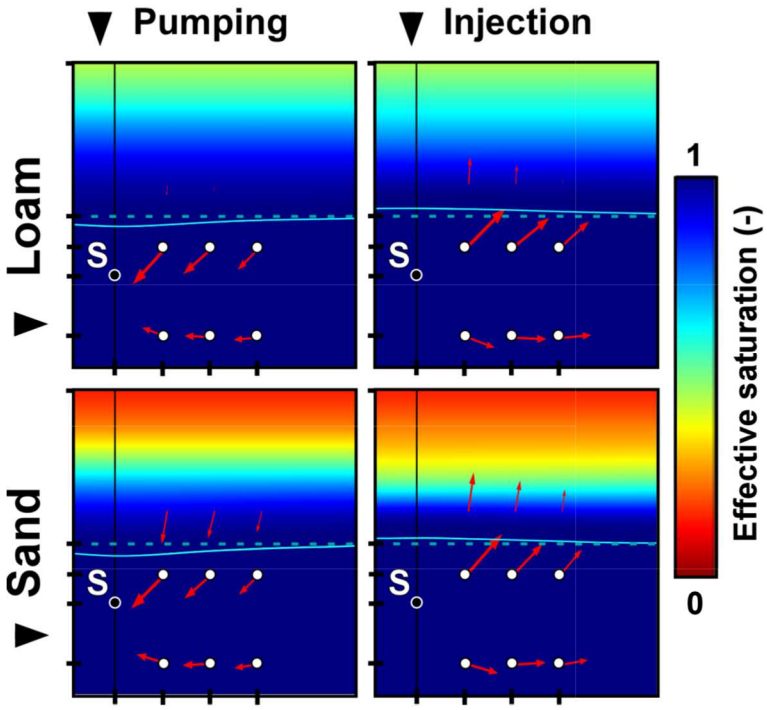

Figure 4: Flow velocity vectors (red arrows) in a log10 scale when pumping and injecting in loam or in sand. Current and initial saturation levels are indicated as blue lines and dotted lines respectively.

We first evaluated how oscillatory responses (i.e., amplitudes, phase lags) are affected by variations of individual parameters values for the intermediate soil (Table 1) using a pumping amplitude of $Q_A = 1$ mL/s and period of oscillation $Pe = 15$ min.

In Figure 5, we present the variations induced in the amplitude and phases responses at the different locations when modifying the conductivity and anisotropy values of our 'intermediate' soil (to values corresponding rather to 'sand' soil ones or rather to 'loam' soil

ones). The absolute responses (presented for the ‘intermediate’ soil in the middle column of the figure) globally show an amplitude decrease and phase increase with the radial distance to the perturbation source point S. However the oscillation better propagates in the deep saturated zone (below S) than near the unsaturated one, as amplitudes are higher and phases lower below S, even if these simulation points are more distant to the source than the ones above S. It clearly appears that the oscillatory responses are affected by the conductivity and its anisotropy, especially in terms of amplitudes. For a similar perturbation the amplitude responses will be higher in loam than in sand. Oppositely, the phases will become globally lower when applied in loam and higher in sand. However, in this case the conductivity seems to more particularly affect the phases of responses associated to horizontal flows (below S). The degree of anisotropy will have a similar but less important effect than conductivities on amplitude responses, becoming more important in loam with higher anisotropy. The phase responses are especially affected when lowering the anisotropy, generating higher phases in sand when moving away from the perturbation source.

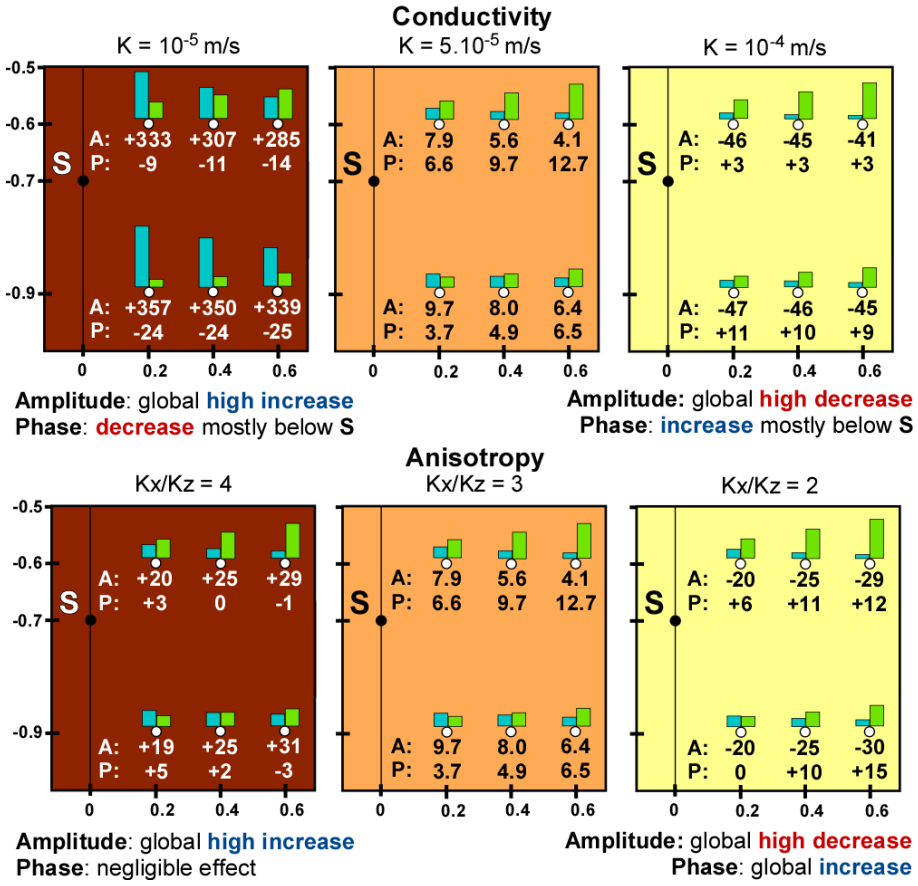

Figure 5: Lateral columns: spatial variations (in %) of amplitudes (blue, A) and phases (green, P) at each measurement point and for the saturated flows properties (K and anisotropy) tending to their 'sand' soil or 'loam' soil values. Middle column: absolute amplitude (in mm) and phase responses (in °) obtained with medium property values of the 'intermediate' soil.

Figure 6 presents a similar analysis with the Van Genuchten parameters α and n, associated to the unsaturated flows. These parameters also affect the oscillatory responses, but in a different manner than conductivity. Parameter α appears to affect the differences in the responses above and below S. In fact, its modification will generate more important variations in terms of amplitude above S (denoting an effect on the vertical flows impacts). It will also affect the phase responses but rather reducing the vertical differences in loam, and accentuating it in sand, thus, again, generating responses variations vertically. Parameter n, in contrary, generates variations affecting essentially the phases of the responses, accentuating them and their vertical differences in loam and lowering them in sand. The phase variations

255 remain constant with distance to S. This suggests a more local impact at the perturbation point
256 that is then propagated to the other responses. As for the previous conductivity analysis, the
257 effects on the responses induced by α and n are opposites when tending to one or another
258 sand or loam property value. This already suggest that quantitatively analyzing the responses
259 spatially and vertically could allow to assess a soil's saturated and unsaturated hydraulic
260 property values.

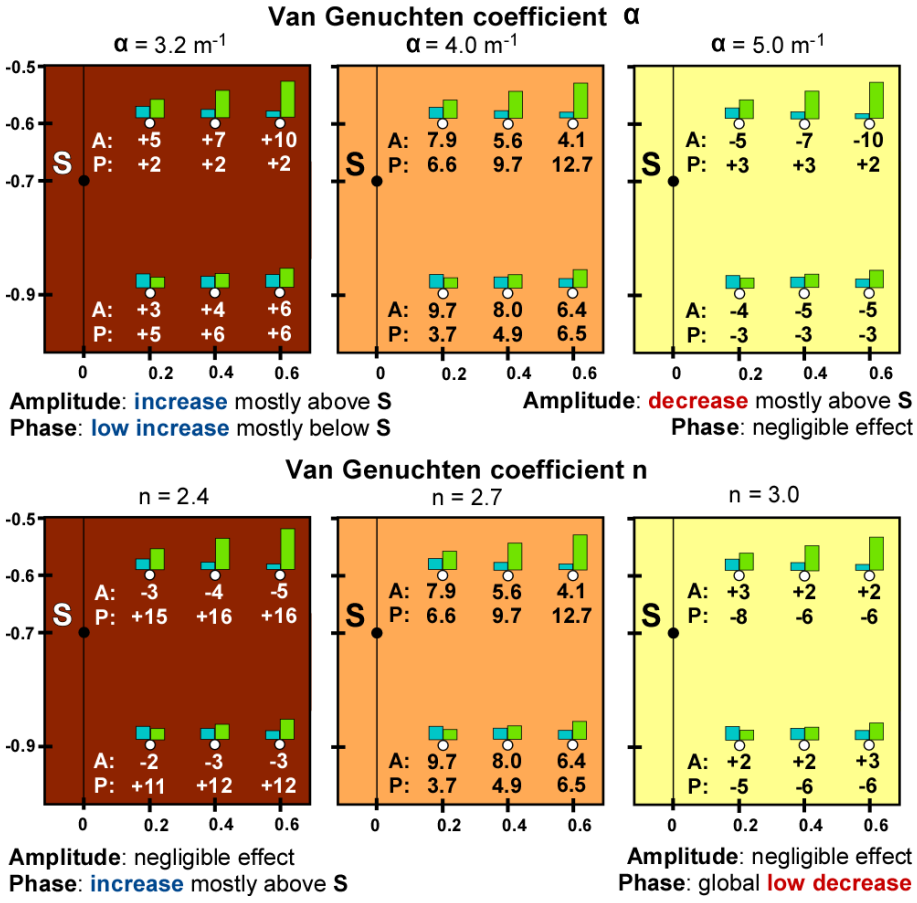

261

262 Figure 6: Lateral columns: spatial variations (in %) of amplitudes (blue, A) and phases (green,
263 P) at each measurement point and for the unsaturated flows properties (α and n) tending to
264 their 'sand' soil or 'loam' soil values. Middle column: absolute amplitude (in mm) and phase
265 responses (in °) obtained with medium property values of the 'intermediate' soil.

266

267 A third similar analysis has been conducted on other parameters, not necessarily linked to the
268 two types of soil (loam and sand) considered in this study. This analysis is presented in Figure
269 7 with the effect of the period of oscillation, the saturated water content of the soil and the

magnitude of hysteresis effect. The period of oscillation influences the distance of propagation of the perturbation in the soil. A lower period will attenuate more rapidly with distance to S. An opposite effect is observed when increasing the period. A vertical effect of the period can also be observed. The period tends to accentuate the vertical difference observed in the responses above and below S when it is decreased (more important horizontal flows), and to reduce this difference for higher periods. The saturated water content generates a similar effect, but with opposite variations. In fact, a higher saturated content will accentuate the vertical differences in the responses, while a lower saturated content will reduce the vertical differences. The hysteresis effect occurring in the unsaturated zone does not substantially affects the oscillatory responses in the considered range of periods of oscillation (5 to 30 min) except a global low increase of the phase responses that can be observed for a high hysteresis magnitude. Nevertheless, Figure 2 shows that this effect affects the mean saturation level over time. However, when performing a FFT analysis on the pressure responses, this mean level can be isolated.

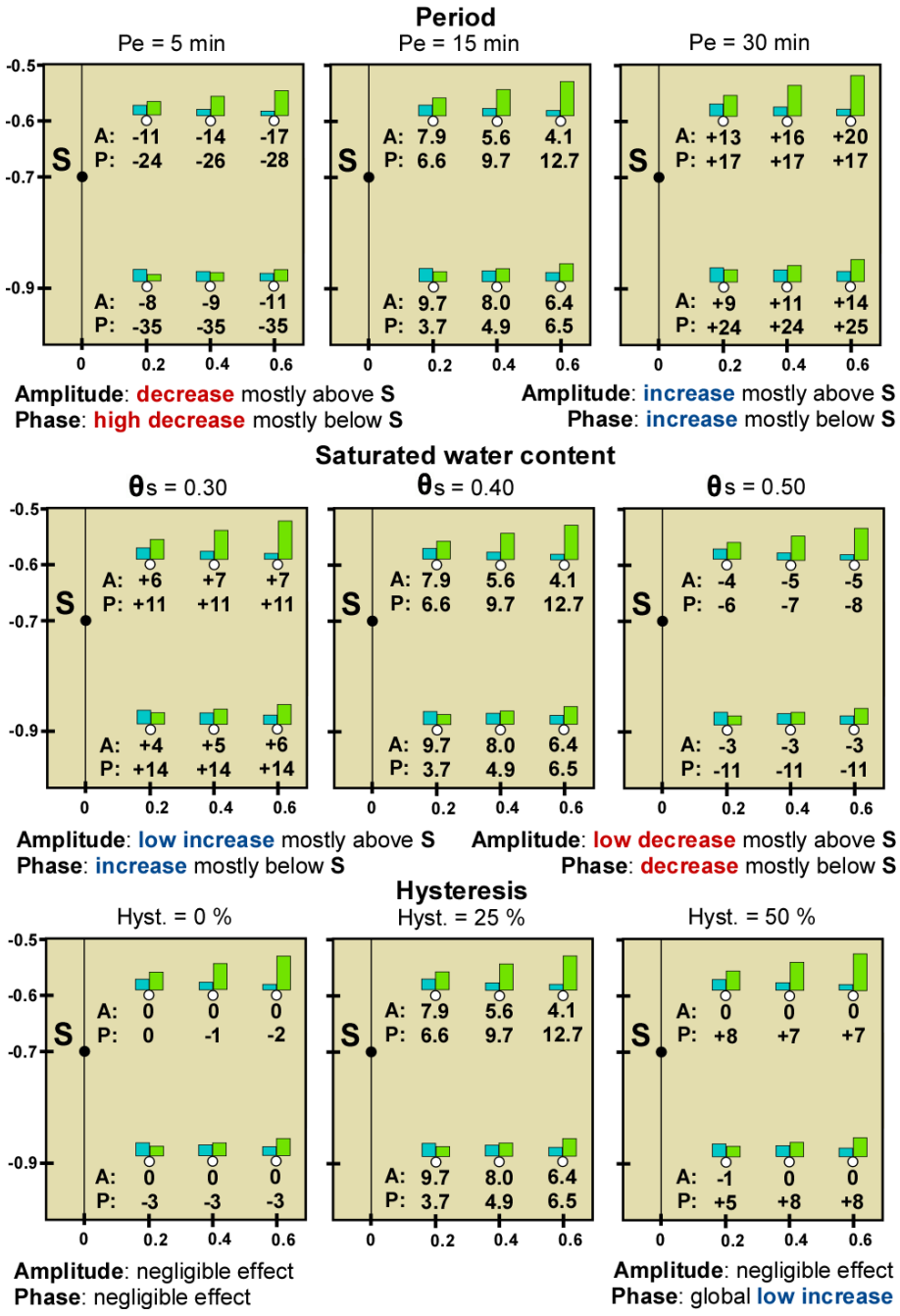

284

285 Figure 7: Lateral columns: spatial variations (in %) of amplitudes (blue, A) and phases (green,
286 P) at each measurement point and for different parameters (oscillation period, hysteresis
287 magnitude and saturated water content) tending to minimal and maximal values. Middle
288 column: absolute amplitude (in mm) and phase responses (in °) obtained with medium
289 parameter values between these extrema.

290

291 This first comparative analysis shows that the spatial oscillatory responses are differently

292 affected by the different soil properties and signal parameters. One advantage of oscillatory

responses is that they can be easily dissociated into amplitudes and phases, which are also differently affected by each properties. Therefore, this type of responses could be used to assess the values of different soil properties.

4. Imaging potential of the oscillatory responses in the saturated zone

4.1. Inverse problem

In order to analyze if, and how, responses to oscillatory signals may provide information in order to image the spatial distribution of hydraulic properties in an aquifer, we have re-interpret generated oscillatory responses in our 'sand' or 'loam' soils models through inversion processes. The inverse problem is based on objective functions, which quantify the gap between responses simulated through a physical model for given property values and a set of observed responses that one wants to interpret. These objective functions also incorporate a priori information on the property values in order to overcome the issue of non-unicity of the solution.

We use our model presented in section 2 to generate oscillatory responses for different values of conductivities K and Van Genuchten parameters α and n. This operation can be mathematically written:

$$\mathbf{d} = f(\mathbf{p}) \tag{8}$$

where $\mathbf{d}$ is a $(n \times 1)$ vector containing the amplitude and phase responses simulated at each measurement location, f is the solver of the numerical model and $\mathbf{p}$ is a $(m \times 1)$ vector containing distributed values of K, α and n in logarithmic scale. Using logarithmic values permits avoiding negative values during the optimization process.

A simultaneous optimization of different properties in the iterative inversion process can lead to a divergence of the process. Furthermore, as shown in previous section, the amplitude

316 responses appear to be especially sensitive to conductivity. Therefore, we decided to perform
317 our inversion process sequentially, with two different objective functions Ψ_K and $\Psi_{\alpha,n}$, that
318 are conceived to successively optimize the hydraulic conductivity K, only with the amplitude
319 responses, and then the Van Genuchten parameters α and n by adding the phase responses in
320 the process:

321 $$\Psi_K = \left(\mathbf{d}_{amp}^{obs} - \mathbf{d}_{amp}\right)^T .\mathbf{R}_{amp}^{-1}.\left(\mathbf{d}_{amp}^{obs} - \mathbf{d}_{amp}\right) + \left(\mathbf{p}_K^{prior} - \mathbf{p}_K\right)^T .\mathbf{C}_K^{-1}.\left(\mathbf{p}_K^{prior} - \mathbf{p}_K\right) \quad (9)$$

322 $$\Psi_{\alpha,n} = \left(\mathbf{d}^{obs} - \mathbf{d}\right)^T .\mathbf{R}^{-1}.\left(\mathbf{d}^{obs} - \mathbf{d}\right) + \left(\mathbf{p}_{\alpha,n}^{prior} - \mathbf{p}_{\alpha,n}\right)^T .\mathbf{C}_{\alpha,n}^{-1}.\left(\mathbf{p}_{\alpha,n}^{prior} - \mathbf{p}_{\alpha,n}\right) \quad (10)$$

323 where Ψ designates the objective functions for determining K or α and n from the
324 information carried by the amplitude and phase responses contained in a n-vector $\mathbf{d}^{obs}$.
325 $\mathbf{R} = \sigma^2.Id(n)$ is a $n \times n$ diagonal matrix holding variances σ^2 on the amplitude ($\sigma^2 = 0.1$
326 cm) and phase responses ($\sigma^2 = 1°$). $\mathbf{d}_{amp}^{obs}$ and $\mathbf{R}_{amp}$ designate the sub-vector and sub-matrix
327 associated only to the amplitude responses. $\mathbf{p}^{prior}$ is a m-vector containing a priori values of
328 K (in sub-vector $\mathbf{p}_K^{prior}$) and α and n (in sub-vector $\mathbf{p}_{\alpha,n}^{prior}$). $\mathbf{C}$ is a $m \times m$ matrix holding
329 covariances constraining the hydraulic property values and their distribution. $\mathbf{p}_K$, $\mathbf{p}_{\alpha,n}$, $\mathbf{C}_K$
330 and $\mathbf{C}_{\alpha,n}$ designate the sub-vectors and sub-matrices associated to K or α and n.

331 The inversion process consists in an iterative process aiming to minimize the values of these
332 objectives function successively, by updating deterministically the property values in the
333 model via the computation of a Jacobian matrix (Tarantola and Valette 1982):

334 $$\mathbf{F}_i = \frac{f_i\left(\mathbf{p}_j + \Delta p\right) - f_i\left(\mathbf{p}_j\right)}{\Delta p} \quad (11)$$

where $\mathbf{F}_i$ represents the sensitivity of a data i to modification $\Delta p = 10^{-2}$ on the property value j.

During the first inversion sequence, the update of the conductivity values from an iteration $k-1$ to k is given by:

$$\mathbf{p}_K^k = \mathbf{p}_K^{k-1} + \left(\mathbf{F}_K^T.\mathbf{R}_{amp}^{-1}.\mathbf{F}_K + \mathbf{C}_K^{-1}\right)^{-1}.\left(\mathbf{F}_K^T.\mathbf{R}_{amp}^{-1}.\left(\mathbf{d}_{amp}^{obs} - \mathbf{d}_{amp}\right) + \mathbf{C}_K^{-1}.\left(\mathbf{p}_K^{prior} - \mathbf{p}_K\right)\right) \quad (12)$$

where $\mathbf{F}_K$ is the Jacobian matrix described in Eq. 11, performing the sensibility analysis between the K values and amplitude responses.

During the second inversion sequence, the update of the Van Genuchten parameters values from an iteration $k-1$ to k is given by:

$$\mathbf{p}_{\alpha,n}^k = \mathbf{p}_{\alpha,n}^{k-1} + \left(\mathbf{F}_{\alpha,n}^T.\mathbf{R}^{-1}.\mathbf{F}_{\alpha,n} + \mathbf{C}_{\alpha,n}^{-1}\right)^{-1}.\left(\mathbf{F}_{\alpha,n}^T.\mathbf{R}^{-1}.\left(\mathbf{d}^{obs} - \mathbf{d}\right) + \mathbf{C}_{\alpha,n}^{-1}.\left(\mathbf{p}_{\alpha,n}^{prior} - \mathbf{p}_{\alpha,n}\right)\right) \quad (13)$$

where $\mathbf{F}_{\alpha,n}$ is the Jacobian matrix described in Eq. 11, performing the sensibility analysis between the α and n values and amplitude and phase responses.

At the end of the inversion, the standard deviations on the inverted property values can be obtained from the square-roots values of the diagonal entries of matrix $\mathbf{C}^{post}$, using the last iterations Jacobian matrices:

$$\mathbf{C}^{post} = \left(\mathbf{F}^T.\mathbf{R}^{-1}.\mathbf{F} + \mathbf{C}^{-1}\right)^{-1} \quad (14)$$

Performing an inversion in this way, by isolating the K values in the process, we could improve the stability of the inversion and accelerate its convergence to more realistic solutions. In fact, the results presented hereafter show that the amplitude responses can be closely reproduced by optimizing the K field, regardless of the Van Genuchten parameters. The remaining amplitude and phase differences can then be adjusted by optimizing the Van

356 Genuchten parameters. In fact, we have also tested inversions simultaneously optimizing K,
357 α and n that did not converge. In particular it seems that a good assumptions on K is
358 required prior to the optimization of the Van Genuchten parameters.

359 For all inversion applications presented hereafter we did not consider any hysteresis effect on
360 the responses simulated in the inversions, even if the observed data were generated with a
361 25% hysteresis magnitude.

362 ## 4.2.Homogeneous cases applications

363 Inversions have been performed with oscillatory responses generated in homogeneous loams
364 or sands (using property values presented in Table 1). For this generation we applied an
365 injection/extraction rate aiming to generate similar pressure amplitudes (10 cm) at the
366 perturbation point in both type of soil (i.e. $Q_A = 1$ mL/s in loam and $Q_A = 10$ mL/s in sand).
367 The generated responses have been noised (2% added noise) for the imaging applications.

368 The hydraulic properties were optimized within two blocks (one 'superficial' block between 0
369 and 65 cm depth and one 'deep' block between 65 and 100 cm depth). Thus, in our inversions
370 the number of property values to be inverted was $m = 6$ (2 distributed values for each
371 property) for a dataset composed of $n = 7$ amplitude/phase responses couples. We considered
372 a diagonal covariance matrix for $\mathbf{C}$ with a 0.01 variance on each property value. We
373 initialized our inversions with the 'medium' soil properties (see Table 1) so that we would be
374 able to estimate if the information carried by the oscillatory responses would permit to
375 partially or totally recover the loam and sand properties used for their generation. The
376 anisotropy of the medium was considered as known.

377 Figure 8 and Figure 9 present the inversion results obtained with oscillatory responses
378 generated with different oscillation periods (5 and 30 min) respectively in loam and in sand.

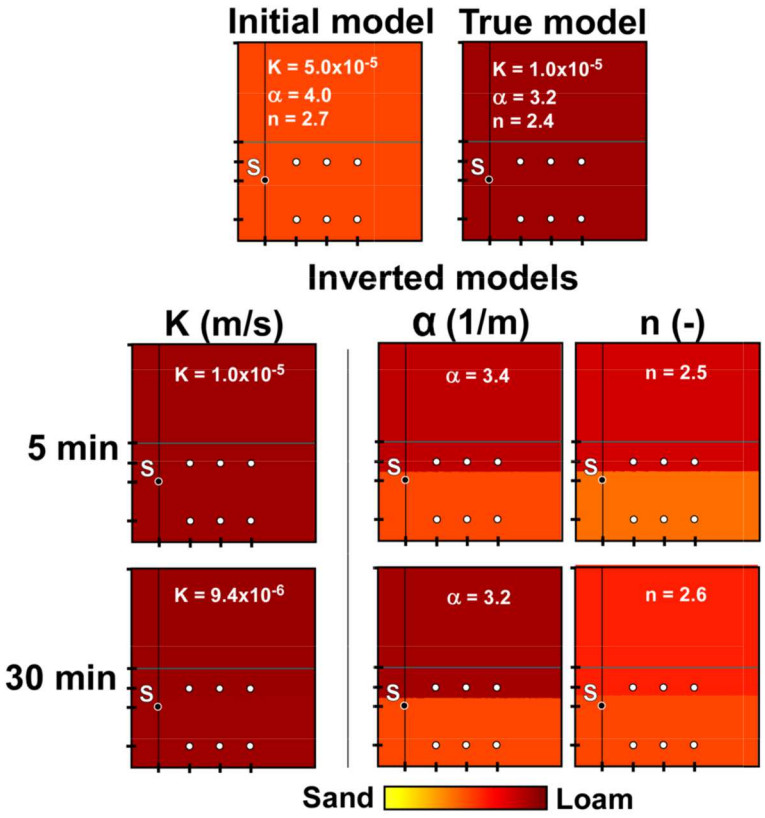

379

380 Figure 8: Inversion results obtained with responses simulated in a homogeneous loam with
381 different periods of oscillations (5 and 30 min). Conductivities are firstly inverted only with
382 the amplitude responses, then the Van Genuchten coefficients are inverted with both
383 amplitude/phase responses.

384

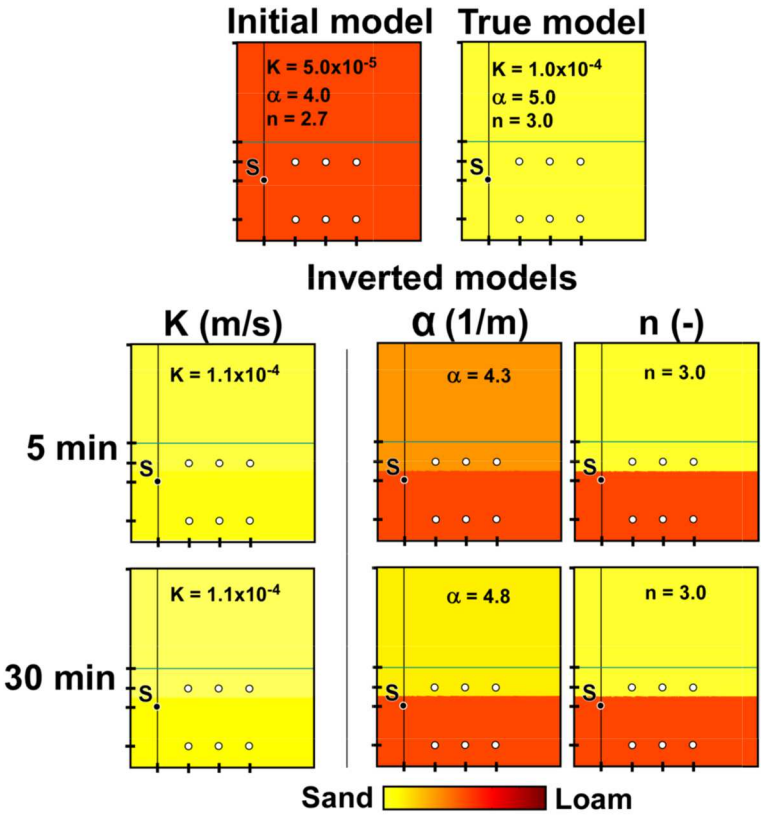

385

386 Figure 9: Inversion results obtained from responses simulated in a homogeneous sand with
387 different periods of oscillations (5 and 30 min). Conductivities are firstly inverted only with
388 the amplitude responses, then the Van Genuchten coefficients are inverted with both
389 amplitude/phase responses.

390

391 Accurate conductivity values can be obtained from the amplitude responses alone, for both
392 type of soils and any oscillation period. A slightly more accurate result is obtained with lower
393 periods. Thus, most of the amplitude responses can be reconstructed by optimizing the
394 conductivities. Then, the remaining responses differences, in terms of amplitudes and phases,
395 can be essentially linked the unsaturated flows and the Van Genuchten parameters.
396 Unsurprisingly, these properties were optimized only in the upper blocks of the models,
397 associated to the unsaturated zone. For α, the accuracy of the characterization seems more
398 period-dependent, better assumptions being systematically obtained with the 30 min periodic
399 responses (i.e. a lower frequency). Regarding n, the accuracy appears to be more related to
400 the soil, with better quantifications obtained in sands rather than in loams.

Globally, we observe that the oscillatory responses measured in the saturated zone provide sufficient information to distinguish the type of soil type in the medium. They can also allow the quantification of accurate properties values associated to the saturated and the unsaturated flows without necessarily having to simulate a hysteresis effect.

4.3.Simplified applications for heterogeneous cases

We have then performed inversions with oscillatory responses simulated in simplistic heterogeneous cases (see Figure 10) in a wider sandbox (3.6 m width). These cases consisted in 3 perturbations points (black dots in Figure 10) in a 'medium' soil (as described in Table 1), surrounded by sand or loam areas in the saturated or unsaturated zones. The velocity vectors simulated at each observation point (white dots in Figure 10) show that the generated flows are differently affected in each areas of the model. Most important velocities are observed in the sand areas, both in saturated and unsaturated zones. Therefore, in order to efficiently characterize the whole heterogeneity, it is necessary to cross-interpret data generated by signal sources located at different locations (hydraulic tomography principle).

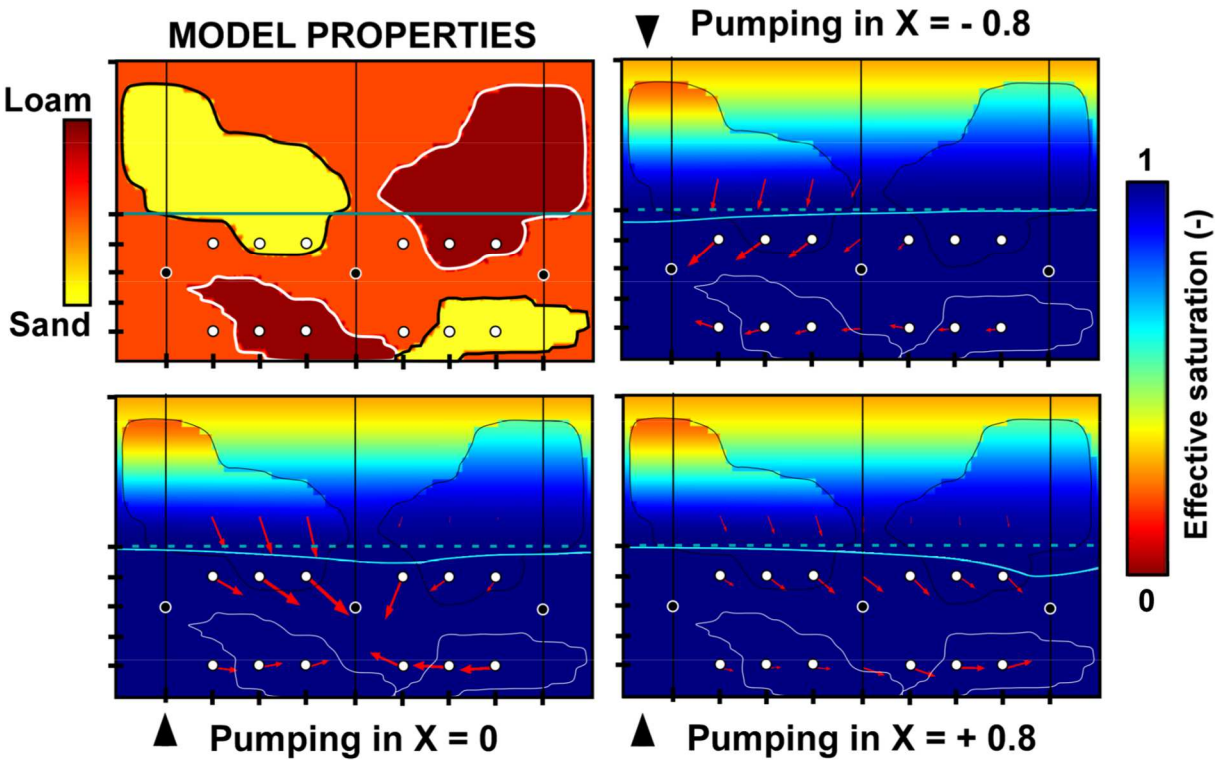

Figure 10: Flow velocity vectors (red arrows) in a log100 scale when pumping at different locations (X=-0.8, X=0 and X=+0.8) in the heterogeneous model (shown in the upper left corner). Current and initial saturation levels are indicated as blue lines and dotted lines respectively.

Thus, for the inversions we have simultaneously inverted the responses generated with each of the three perturbation sources. These responses have been noised (2% added noise) for the imaging applications. We considered the anisotropy of the medium and also the properties of the soil at the perturbation locations to be known. We have performed two types of inversions. In a first inversion we have considered having a certain prior knowledge on the existing contrast in the soil, and therefore invert properties within delineated zones. In a second inversion, we did not consider this knowledge and inverted the properties within a grid regularly distributed in 2D in the saturated zone and in 1D in the unsaturated zone (see dotted lines delineations in Figure 12).

For our zoned inversions the number of property values to be inverted was $m = 12$ (4 zoned values for each property) for a dataset composed of $n = 45$ amplitude/phase responses couples (15 responses obtained for each perturbation). We considered a diagonal covariance matrix for $\mathbf{C}$ with a 0.01 variance on each property value. We have tested different combinations of responses generated with lower or higher periods of oscillation (5, 15 or 30 min) in terms of imaging efficiency, and for different heterogeneity configurations (3/4 sand, 3/4 loam and half sand/half loam). The best imaging results obtained are presented in Figure 11.

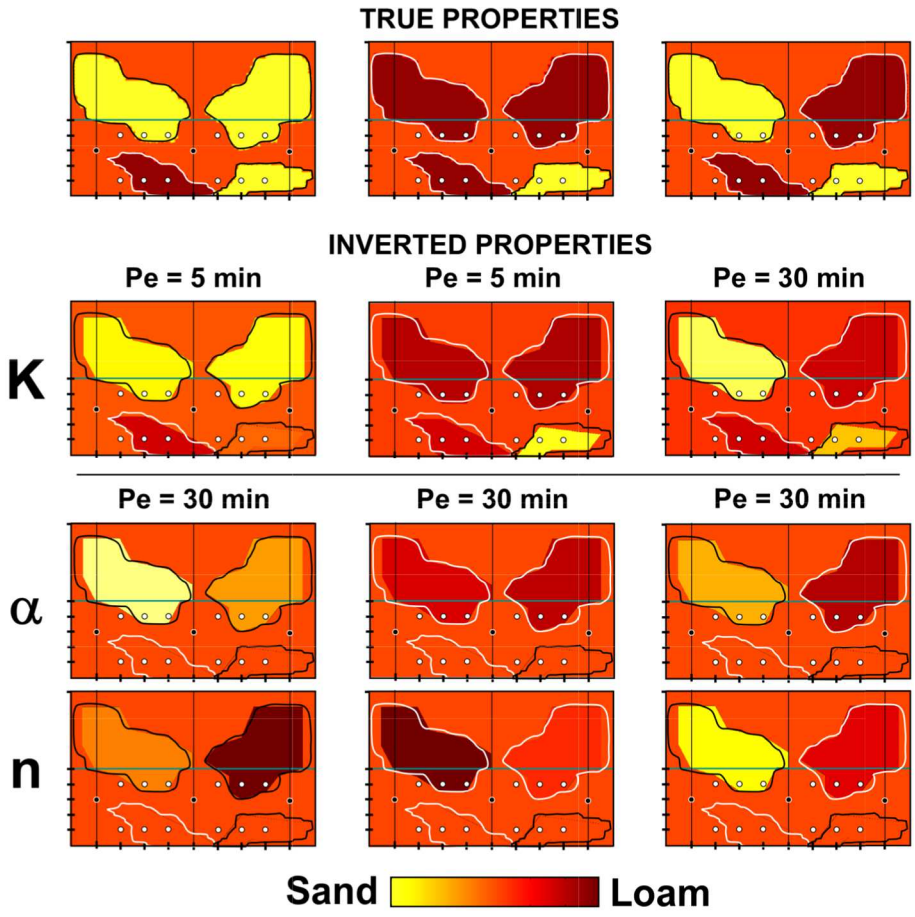

437

438 Figure 11: Results obtained for the best inversion configurations with responses simulated in
439 heterogeneous soils with different periods of oscillations (5, 15 and 30 min). Conductivities
440 are inverted only with the amplitude responses, while the Van Genuchten coefficients are
441 inverted with both amplitude/phase responses.

442

443 Here again, amplitude responses alone are sufficient to reconstruct the heterogeneous contrast
444 in the conductivity field for each period of oscillation tested. The inverted conductivity
445 values, however do not always exactly match the true ones. It appears that a contrasted soil
446 (half sand/half loam zones) is better characterized with higher periods of oscillation, while a
447 less contrasted medium is better characterized with lower periods. Concerning the Van
448 Genuchten parameters, optimized with the remaining differences in the amplitude and phase
449 responses that could not be reproduced with conductivity alone, they are better characterized
450 with the higher period of oscillation in each case. As for the homogeneous cases, they can be
451 characterized only in the unsaturated zone of the soil and do not image heterogeneities in the

saturated zone. Parameter α appears to be more reliable than n for the interpretation of heterogeneity in the capillary fringe. In fact, in our results, inverted n values are good for the upper left zone, but not always for the upper right one, while α values are always coherent in both corners.

For our distributed inversions the number of property values to be inverted was $m = 123$ (41 distributed values for each property). We constrained the spatial distribution of the inverted property values with an exponential variogram model with a range of 2 to compute the covariance values in matrix $\mathbf{C}$. We inverted the responses generated in the half sand/half loam heterogeneous configuration with a period of oscillation of 30 min (according to the best result configuration in the zoned inversions). The inverted property fields and their associated normalized standard deviations are presented in Figure 12.

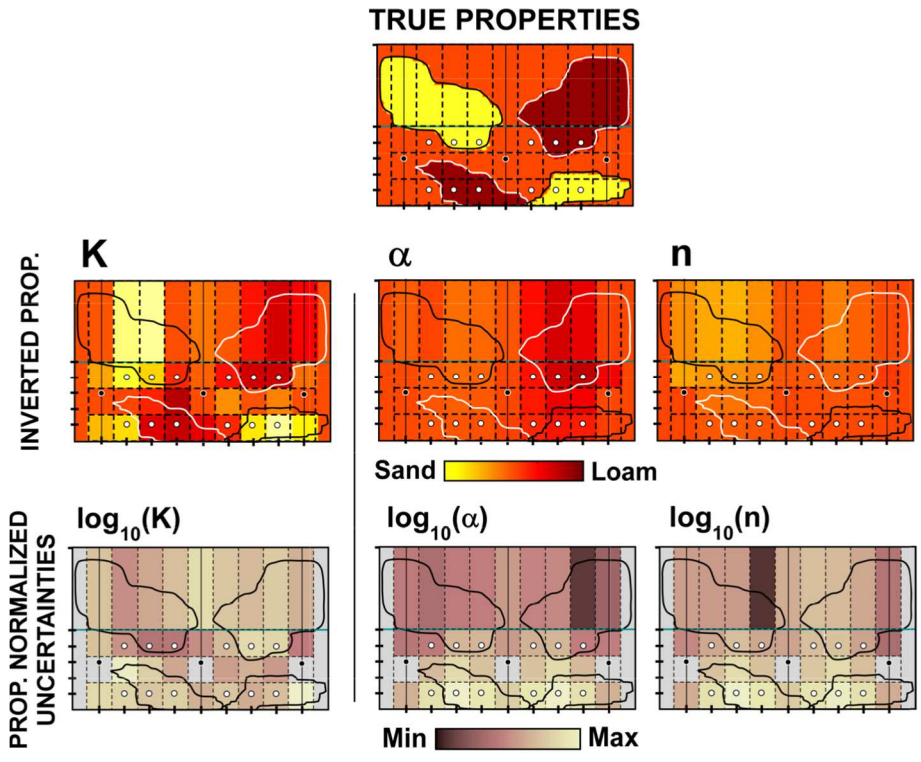

Figure 12: Property values and their associated normalized standard deviations obtained from the inversion of amplitudes (for K) and amplitudes/phases (for α and n) responses generated in an heterogeneous soil (true properties) solicited with 30 min period oscillations. The inversion grid is delineated with dotted lines.

The inverted property values globally do not match the true ones, they are mostly underestimated. This can be explained by the lack of spatial constraints in this inversion that allows optimization process to generate local equivalent property values for the reproduction of the data, especially for K, which is optimized first. However, the trends and localizations of the heterogeneous contrasts can be imaged in both the saturated and unsaturated areas in the conductivity field. The conductivity field is mainly sensible to the sand zones in the saturated area, according to the distribution of its uncertainties. On the other hand, again unsurprisingly, the Van Genuchten parameters image only the heterogeneities in the unsaturated area. However, in this distributed inversion it appears that α rather image the loam areas, while n rather image the sand areas. The uncertainty analysis shows a globally higher local sensitivity, near the perturbation sources for n, and a more homogeneous sensitivity among the whole unsaturated area for α.

5. Discussion

5.1.Effects of hydraulic properties on the saturated responses

Our hydraulic analysis, presented in this article, tends to indicate that the different hydraulic properties considered K, α and n affect differently the measured oscillatory responses in the saturated zone and that their relation to such type of responses is also conditioned to different factors, such as the depth of the source or the measurement locations.

The conductivity K globally appears as the most interesting hydraulic property to be characterized with oscillatory responses. In fact, it is highly linked to the amplitude of the responses, more than the other studied properties, and, thus, can be easily isolated from these other properties when analyzing the responses. Basing our inversions of K on the amplitudes alone resulted, indeed, in good characterizations of its distributions in each configuration,

even without considering accurate Van Genuchten parameters. This observation is in agreement with other works on unconfined media. Huang et al. (2019) analyzed the sensitivity of oscillatory responses in unconfined aquifers through an analytic solution and noted the same high sensibility of the responses to K. However this observation does not seem specific to oscillatory data. In fact, in their hydraulic tomography applications taking account unsaturated flows, Mao et al. (2013b) and Zhao et al. (2015) also observed that the contrasts in conductivity fields could be globally well imaged with responses to constant-rates pumping. Mao et al. (2013b) even noticed the same fact that saturated flows properties could be well characterized even without accurate guesses on the unsaturated ones.

Concerning the Van Genuchten parameters, there is currently no previous studies taking them into account in a characterization of an unconfined aquifer with oscillatory signals. Mao et al. (2013b) and Zhao et al. (2015) employed the Gardner-Russo's model to simulate the unsaturated flows and found that its parameters could be well characterized only in the unsaturated area. In our study we observed that the oscillatory responses in the saturated zone are affected by both α and n, with various intensities depending on the period of oscillation, the type of soil and the type of flows generated. The effect of n appears to be more related to the local response at the perturbation source (local fluxes), while α generates a more distributed effect on the responses (vertical flows affecting the whole capillary fringe). The imaging potential of α, therefore, appears as more reliable at the scale considered in our results (metric scale). Trying to link this hydraulic behavior to geological explanations is a complex topic that is discussed in the literature. It is mainly accepted that α is related to the air entry suction of the soil and n to the distribution of the pore size. Benson et al. (2014) observed that, for a uniform sand, the breadth of the particle size influenced n, while α was more linked to a median value of the particle size, indicating a more integrative effect. Porebska et al. (2006) noted that n was directly dependent to their soil composition (sand,

clay, silt), which we also observe in our results, while parameter α appeared to be more related to the granulometry of the sample.

5.2. Advantages of oscillatory signals and period-dependent effects

Separating the responses signals into amplitude and phase allow for a better separation of the information contained in the data. Absolute amplitudes can be used to specifically characterize the conductivity K and appear to carry already a sufficient amount of information to interpret its variations around the perturbation points, which can then be used to guide the characterization of the unsaturated flows parameters. This possibility of separating the responses into amplitudes and phases in real cases can be achieved only if the responses reach a simple harmonic motion, mainly after several periods. The conditions allowing to reach this conditions are described in Bakhos et al. (2014) and in Huang et al. (2019). Oscillatory signals also offers the possibility to be easily extractable from other sources of signals or noises. Techniques to efficiently process field oscillatory responses are proposed in Bakhos et al. (2014). It can also be noted that oscillatory responses generated with wetting/dewatering of an unsaturated soil potentially allow to assess mean values of α and n in the water content curves, while responses associated to constant pumping would characterize only the Van Genuchten values associated to the dewatering part of the curve due to the hysteresis 'scanning loops' effect.

The effect of the period of oscillation on the flows generated in an aquifer has been discussed in previous works (Rabinovich et al. 2015; Cardiff et al. 2013b; Fischer et al. 2018; Fischer et al. 2020b). Globally, according to these works, decreasing the period of oscillation accentuate flows in the most conductive and mobilizable areas of the field and in the vicinity of the pumping/injection location. As water in the unsaturated zone represents a less mobilizable source of water than the volume in the saturated area, it appears as logical that a lower period

of oscillation accentuate the horizontal flows and does not allow for a good characterization of the unsaturated area. In their field applications, Rasmussen et al. (2003) observed, in fact, that with a very low period of oscillation, the responses generated in an unconfined aquifer could be assimilated to confined-medium responses. Therefore, low periods of oscillations may be employed with care for unconfined aquifers according to several previous works on this topic (Rasmussen et al. 2003, Rabinovich et al. 2015; Cardiff et al. 2019). Cardiff et al. (2019) also suggested that, for high frequencies (period < 1 min), the existing models such as the Richards-based may become inaccurate.

According to our results, if lower periods provided better imaging results for K when the medium was homogeneous or with lowly contrasted heterogeneities, a higher period of oscillation should be adopted if one wants to characterize draining effects parameters, especially for α (n being more related to local responses seems less dependent to the period). However, when dealing with higher period signals, hysteresis effects should be considered with unsaturated flows. In our results, for periods between 5 and 30 min and at a metric scale, we show that we can neglect its effects on the responses (only for the responses in the saturated zone). Experiments made in Cartwright (2014) and Shoushtari et al. (2015) are in agreement with this observation when the period of oscillation remain relatively low. However the authors noted that for high periods of oscillations reaching several hours or more, the hysteresis effect could become important even on the responses in the saturated zone and should be taken into account.

5.3.Toward real cases

The analysis proposed in this article represents a preliminary work for future real cases tomographic applications. It remains theoretical and real cases applications would face other problematics not considered in our models, such as the impact of environmental noise on the

565 data. However, it provides some information and methods that may be helpful for a better
566 setup of oscillatory data interpretation in an unconfined aquifer.

567 A first adaptation for a field application would be to consider 3-D flows with boundary
568 conditions often not affecting the perturbed volume. Therefore we have also simulated flows
569 in a cylindrical homogeneous model with a similar geometry but a constant head boundary
570 condition located far away from the perturbation source point S (50 m away). This
571 configuration thus considers volumetric effects and a theoretical infinite volume (as water can
572 enter or leave the model through the constant head boundary). These consideration are more
573 realistic for a field case. We compare the responses simulated in this way in sand and loam to
574 our 2-D model previously discussed in Figure 13. In order to generate a signal of similar
575 amplitude at the perturbation source it is necessary to increase its flowrate amplitude (40
576 times in loam, 30 times in sand). However, the spatial responses simulated in this way will be
577 different from the ones obtained in the 2-D finite-volume model: the attenuation of amplitude
578 responses and the phase lags increase with distance become more important in the cylindrical
579 infinite-volume model. In order to generate responses in the cylindrical model that are closer
580 to the 2-D ones, it is necessary to also increase the period of oscillation and the signal source
581 depth (relatively more in loam than in sand). If the adopted cylindrical model remains very
582 simplistic compared to real field, it permits to provide insights on what configuration
583 parameters should be especially considered for fields applications (i.e. flowrate amplitude,
584 signal source depth and oscillation period) and how to adapt to different type of soils.

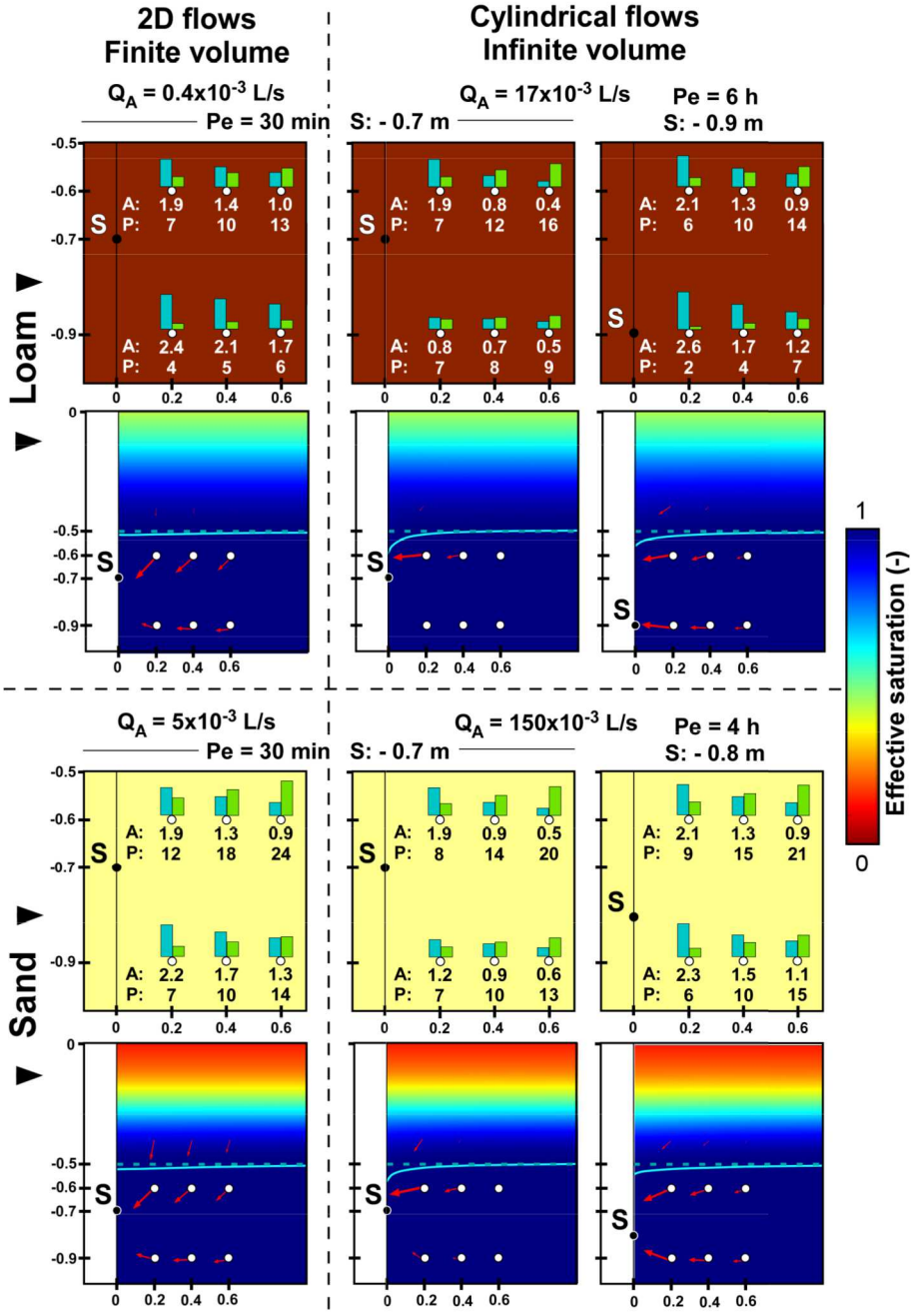

585

586 Figure 13: Observed amplitude (A in cm) and phase (P in °) responses and simulated
587 saturated interface during pumping phase in homogeneous sand or loam considering either 2D
588 flows in a finite volume or cylindrical flows in an infinite volume and different signal
589 amplitudes (Q_A), depths (S) and periods (Pe).

590

591 ## 5.4.Imaging potential in tomographic applications

592 According to the results presented in this work, having measurements and perturbation
593 locations distributed spatially and also at different depths of the aquifer might provide
594 different information on the different hydraulic properties. Horizontal flows effects might be
595 better characterized by deeper responses or perturbation, while the vertical flows effects can
596 be better characterized by perturbation and measurements near the unsaturated zone. This
597 accumulation of distributed perturbations and information is, furthermore, a well-known and
598 widely used technique for the characterization of aquifers in hydraulic tomography.
599 Furthermore, we could observe that the localization of the signal source in depth was crucial
600 for the characterization of the unsaturated area. It is, in fact, necessary to generate a
601 movement of the saturated/unsaturated interface, in order to generate vertical flows, mainly
602 with a source close to this interface, or at this interface directly (such as tide periodic sources).
603 Mao et al. (2013a) provided several conditions on the dataset to perform accurate hydraulic
604 tomography of unconfined aquifers. In particular they recommend to measure fluxes in
605 addition to pressure data and to couple different type of data in order to better characterize the
606 heterogeneity of the medium. Ideally, the different data should also identify flow processes in
607 the saturated and the unsaturated zone separately. Coupling geophysical data, allowing to
608 image water content variations in the soil and heterogeneity contrasts, could greatly improve
609 the imaging results. Indeed, our inversions constrained with zones (that can be typically
610 delineated from geophysical interpretations) showed better results than the regularly
611 distributed ones.

612 In the method and the imaging applications presented in this work, we consider prerequisites
613 knowledges on the properties. In particular we assume the storage coefficient, the anisotropy,
614 and the saturated and residual water content of the medium to be known. Therefore, for a real
615 application case using the inversion method proposed in this paper, one would need to
616 estimate these values. For this purpose, Cheng and Renner (2018) proposed analytical

617 solutions comparing pressures amplitude and phase responses measured above and below an
618 oscillatory source to its flow-rate signal allowing to estimate the anisotropy and storage
619 coefficient at the perturbation location. These solutions provide local estimates that can then
620 be used for the imaging application. However, even if the storage coefficient remains
621 unknown it is possible to image diffusivity ($D = K/S_S$), thus inverting K and S_S together.
622 Estimations of water contents constants would be more complicate in field applications, but
623 important impacts on the oscillatory responses can be observed only for large variations in
624 their values, according to our analysis in section 3. Thus, an average guess may be sufficient
625 for an imaging application.

626 ## 6. Summary and conclusion

627 This article presents a numerical analysis for the hydraulic interpretation of oscillatory
628 responses measured in an unconfined media at a metric scale and including the effect of the
629 capillary fringe. It represents a useful preliminary work for future real cases tomographic
630 applications in unconfined media (sandbox or field cases), as it permits to point out several
631 comments concerning the characterization of the hydraulic properties K, α and n with such
632 data:

633 1) Conductivity K is highly correlated to the amplitude of the oscillatory responses compared
634 to the other hydraulic properties. Thus, a good characterization of the conductivity
635 distribution in an unsaturated media can be obtained separately with the amplitudes of the
636 responses alone and independently from the unsaturated properties;

637 2) The Van Genuchten parameters α and n, related to unsaturated flows, also affect the
638 responses in the saturated zone. They can be assessed, in a second step, from the amplitude
639 and phase responses that could not be reproduced by the previously reconstructed
640 conductivity;

641 3) In a heterogeneous soil, interpreting oscillatory responses in the aforementioned way
642 allows for a coherent reconstruction of the K field (that can then be used to guide the Van
643 Genuchten parameters characterization). The α and n values can be characterized only in the
644 unsaturated zone, and α appears to better image the heterogeneities than n at this scale;

645 4) The period of oscillation of the signal tends to accentuate rather horizontal flows for low
646 periods and generate more vertical flows effects on the responses for high periods. Low
647 periods signals are useful to an accurate assessment of the conductivity values in the saturated
648 area. However, for the characterization of the unsaturated area, high periods of oscillations
649 provide more information but may also be subject to more important hysteresis effects.
650 Nevertheless, for the periods considered in this study (5 to 30 min), these effects could be
651 neglected.

652 These comments may represent interesting advices for real cases applications. However, other
653 problematics not taken into account in this work, might also be considered. Real cases
654 applications are naturally more complex than the model studied in this work, and effect of
655 noise on the measurements also represents a common problematic in such cases. A commonly
656 employed and efficient technique that reduce uncertainties in real field applications is
657 hydraulic tomography. This technique, based on a crossed interpretation of responses to
658 perturbations obtained at several locations and depths, should therefore be considered in
659 association with periodic signals for the spatial characterization of unconfined aquifers
660 properties in future field applications. Addition of other types of data, such as geophysical
661 information could also greatly improve the inversion results in real-cases applications.

662

663 ## Acknowledgments

664 We would like to thank the Region Normandie and EDF R&D for having financially
665 supported this study. We would also like to thank Professor Todd C. Rasmussen, for his
666 valuable comments and suggestions that have helped improve this article.

667 # References

668 Bakhos T., M. Cardiff, W. Barrash, P.K. Kitanidis. 2014. Data processing for oscillatory
669 pumping tests. *Journal of Hydrology* 511: 310-319.

670

671 Benson C.H., I. Chiang, T. Chalermyanont, A. Sawangsuriya. 2014. Estimating van
672 Genuchten Parameters α and n for Clean Sands from Particle Size Distribution Data.
673 Geotechnical Special Publication 233. doi: 10.1061/9780784413265.033.

674

675 Black J.H., K.L. Kipp. 1981. Determination of hydrogeological parameters using sinusoidal
676 pressure tests – a theoretical appraisal. *Water Resources Research* 17: 686-692.

677

678 Cardiff M., W. Barrash, P.K. Kitanidis, B. Malama, A. Revil, S. Straface, E. Rizzo. 2009. A
679 potential-based inversion of unconfined steady-state hydraulic tomography. *Groundwater* 47:
680 259-270.

681

682 Cardiff M., W. Barrash. 2011. 3-D transient hydraulic tomography in unconfined aquifers
683 with fast drainage response. *Water Resources Research* 47: W12518.
684 doi:10.1029/2010WR010367.

685

686 Cardiff, M., W. Barrash, P.K. Kitanidis. 2012. A field proof-of-concept of aquifer imaging
687 using 3-D transient hydraulic tomography with modular, temporarily-emplaced equipment.
688 *Water Resources Research* 48: W05531. doi:10.1029/2011WR011704.

689

690 Cardiff, M., W. Barrash, P.K. Kitanidis. 2013a. Hydraulic conductivity imaging from 3-D
691 transient hydraulic tomography at several pumping/observation densities. Water Resources
692 Research 49: 7311-7326.

693

694 Cardiff M., T. Bakhos, P.K. Kitanidis, W. Barrash. 2013b. Aquifer heterogeneity
695 characterization with oscillatory pumping: Sensitivity analysis and imaging potential. *Water*
696 *Resources Research* 49: 5395-5410.

697

698 Cardiff M., W. Barrash. 2014. Analytical and Semi-Analytical Tools for the Design of
699 Oscillatory Pumping Tests. *Groundwater* 53: 896-907.

700

701 Cardiff M., Y. Zhou, W. Barrash, P.K. Kitanidis. 2019. Aquifer Imaging with Oscillatory
702 Hydraulic Tomography: Application at the Field Scale. *Groundwater*. doi:
703 10.1111/gwat.12960.

704

705 Cartwright N. 2014. Moisture-pressure dynamics above an oscillating water table. *Journal of*
706 *Hydrology* 512: 442-446.

707

708 Cartwright N., P. Nielsen, S. Dunn. 2003. Water table waves in an unconfined aquifer:
709 Experiments and modeling. *Water Resources Research* 39: 1330.
710 doi:10.1029/2003WR002185.

Cartwright N., P. Nielsen, L. Li. 2004. Experimental observations of watertable waves in an unconfined aquifer with a sloping boundary. *Advances in Water Resources* 27: 991-1004.

Cheng Y., J. Renner. 2018. Exploratory use of periodic pumping tests for hydraulic characterization of faults. *Geophysical Journal International* 212: 543-565.

Dagan G., A. Rabinovich. 2014. Oscillatory pumping wells in phreatic, compressible, and homogeneous aquifers. *Water Resources Research* 50: 7058-7066.

Fischer P., A. Jardani, H. Jourde, M. Cardiff, X. Wang, S. Chedeville, N. Lecoq. 2018. Harmonic pumping tomography applied to image the hydraulic properties and interpret the connectivity of a karstic and fractured aquifer (Lez aquifer, France). *Advances in Water Resources* 119: 227-244.

Fischer P., A. Jardani, M. Krimissa, C. Couegnas. 2020a. Hydraulic characterization of a highly anthropized coastal aquifer subject to tidal fluctuations. *Hydrogeology Journal* 28: 2559-2571.

Fischer P., T. De Clercq, A. Jardani, L. Thannberger, N. Massei, M. Abbas. 2020b. Imaging the hydraulic properties of a contaminated alluvial aquifer perturbed with periodic signals. *Hydrogeology Journal* 28: 2713-2726.

Fokker P.A., J. Renner, F. Verga. 2013. Numerical modeling of periodic pumping tests in wells penetrating a heterogeneous aquifer. *American Journal of Environmental Science* 9: 1-13.

Hochstetler D.L., W. Barrash, C. Leven, M. Cardiff, F. Chidichimo, P.K. Kitanidis. 2016. Hydraulic Tomography: Continuity and Discontinuity of High-K and Low-K Zones. Groundwater 54: 171-185.

Huang C.-S., Y.-H. Tsai, H.-D. Yeh, T. Yang. 2019. A general analytical model for head response to oscillatory pumping in unconfined aquifers: effects of delayed gravity drainage and initial condition. *Hydrology and Earth System Sciences* 23: 1323-1337.

Kool J.B., J.C. Parker. 1987. Development and Evaluation of Closed-Form Expressions for Hysteretic Soil Hydraulic Properties. *Water Resources Research* 23: 105-114.

Leij F.J., W.J. Alves, M.T. van Genuchten, J.R. Williams. 1996. Unsaturated soil hydraulic database. UNSODA 1.0 User's Manual. Report EPA/600/R96/095. US Environmental Protection Agency.

753 Lin Y.-C., M.-H. Li, H.-D. Yeh. 2017. An analytical model for flow induced by a constant-
754 head pumping in a leaky unconfined aquifer system with considering unsaturated flow.
755 *Advances in Water Resources* 107: 525-534.

756

757 Liu S., T.-C.J. Yeh, R. Gardiner. 2002. Effectiveness of hydraulic tomography: Sandbox
758 experiments. *Water Resources Research* 38: 1034. doi: 10.1029/2001WR000338.

759

760 Mao D., T.-C.J. Yeh, L. Wan, K.-C. Hsu, C.-H. Lee, J.-C. Wen. 2013a. Necessary conditions
761 for inverse modeling of flow through variably saturated porous media. *Advances in Water*
762 *Resources* 52: 50-61.

763

764 Mao D., T.-C.J. Yeh, L. Wan, J.-C. Wen, W. Lu, C.-H. Lee, K.-C. Hsu. 2013b. Joint
765 interpretation of sequential pumping tests in unconfined aquifers. *Water Resources Research*
766 49: 1782-1796.

767

768 Mishra P.K., V.V. Vesselinov, K.L. Kuhlman. 2012. Saturated-unsaturated flow in a
769 compressible leaky-unconfined aquifer. *Advances in Water Resources* 42: 62-70.

770

771 Neuman S.P. 1972. Theory of flow in unconfined aquifers considering delayed response of
772 the water table. *Water Resources Research* 8: 1031-1045.

773

774 Porebska D., C. Slawinski, K. Lamorski, R.T. Walczak. 2006. Relationship between van
775 Genuchten's parameters of the retention curve equation and physical properties of soil solid
776 phase. *International Agrophysics* 20: 153-159.

777

778 Rabinovich A., W. Barrash, M. Cardiff, D.L. Hochstetler, T. Bakhos, G. Dagan, P.K.
779 Kitanidis. 2015. Frequency dependent hydraulic properties estimated from oscillatory
780 pumping tests in an unconfined aquifer. *Journal of Hydrology* 531: 2-16.

781

782 Rasmussen T.C., R.H. Baldwin, J.F. Dowd, A.G. Williams. 2000. Tracer vs. Pressure Wave
783 Velocities through Unsaturated Saprolite. *Soil Science Society of America Journal* 64: 75-85.

784

785 Rasmussen T.C., K.G. Haborak, M.H. Young. 2003. Estimating aquifer hydraulic properties
786 using sinusoidal pumping at the Savannah River site, South Carolina, USA. *Hydrogeology*
787 *Journal* 11: 466-482.

788

789 Renner J., M. Messar. 2006. Periodic pumping tests. *Geophysical Journal International* 167:
790 479-493.

791

792 Revil, A., C. Gevaudan, N. Lu, A. Maineult. 2008. Hysteresis of the self-potential response
793 associated with harmonic pumping tests. *Geophysical Research Letters* 35:
794 doi:10.1029/2008GL035025.

795

796 Salina Borello E., P.A. Fokker, D. Viberti, F. Verga, H. Hofmann, P. Meier, K.-B. Min, K.
797 Yoon, G. Zimmermann. 2019. Harmonic pulse testing for well monitoring: application to a
798 fractured geothermal reservoir. *Water Resources Research* 55: 4727-4744.

799

800 Shoushtari, A.M.H.J., N. Cartwright, P. Perrochet, P. Nielsen. 2015. Influence of hysteresis
801 on groundwater wave dynamics in an unconfined aquifer with a sloping boundary. *Journal of*
802 *Hydrology* 531: 1114-1121.

803

804 Tarantola A., B. Valette. 1982. Generalized nonlinear inverse problems solved using the least
805 squares criterion. *Reviews of Geophysics* 20: 219-232.

806

807 Yeh T.-C.J., C.-H. Lee. 2007. Time to Change the Way We Collect and Analyze Data for
808 Aquifer Characterization. *Groundwater* 45: 116-118.

809

810 Yeh T.-C.J., C.-H. Lee, K.-C. Hsu, W.A. Illman, W. Barrash, X. Cai, J. Daniels, E. Sudicky,
811 L. Wan, G. Li, C.L. Winter. 2008. A view toward the future of subsurface characterization:
812 CAT scanning groundwater basins. *Water Resources Research* 44: W03301.
813 doi:10.1029/2007WR006375.

814

815 Yeh T.-C.J., D. Mao, Y. Zha, K.-C. Hsu, C.-H. Lee, J.-C. Wen, W. Lu, J. Yang. 2013. Why
816 Hydraulic Tomography Works? *Groundwater*. doi: 10.1111/gwat.12129.

817

818 Zhao Z., W.A. Illman, T.-C.J. Yeh, S.J. Berg, D. Mao. 2015. Validation of hydraulic
819 tomography in an unconfined aquifer: A controlled sandbox study. *Water Resources Research*
820 51: doi:10.1002/2015WR016910.

821

822 Zhu J., T.-C.J. Yeh. 2005. Characterization of aquifer heterogeneity using transient hydraulic
823 tomography. *Water Resources Research* 41: W07028. doi:10.1029/2004WR003790.